

# The EIC reduced cross sections at high inelasticity

G. R. Boroun\*

*Department of physics, Razi University, Kermanshah 67149, Iran*

(Dated: June 3, 2026)

The impact of higher-twist corrections to the ratio  $\frac{\sigma_r}{F_2}(A, Q^2/s, Q^2)$  for light and heavy nuclei is considered at fixed a  $\sqrt{s}$  and  $Q^2$  to the minimum value of  $x$  given by  $Q^2/s$ . The results are for the EIC center-of-mass energies. We apply the influence of higher-twist corrections to  $\frac{\sigma_r}{F_2}(A, Q^2/s, Q^2)$  by the dimensionless variable  $\xi'_A = Q_{s,A}^2/Q^2$  in the color dipole model and obtain bounds for the ratio in the linear region. The importance of contributing to twist-4 at small- $x$  is visible in the linear region where  $\xi'_A \leq 1$ . We perform that twist-4 corrections of the saturation model are shown the successful behavior of  $\frac{F_L}{F_2}(A = 2, x, Q^2)$  in comparison with the JLab data at  $\xi'_A \leq 1$ . The higher-twist corrections due to twist-6 and twist-8 are resummed by the non-linear approaches in the region  $\xi'_A > 1$ . The ratio  $\frac{F_L}{F_2}$  deuteron is considered in the low- $Q^2$  and small- $x$  region and compared with the JLab data which takes into account the non-linear corrections due to twist-6 and twist-8. A comparison with the JLab data shows that the impact of the distinct twists allows us to probe the presence of non-linear effects on the QCD dynamics as  $F_L \rightarrow 0$  and the polarization of the virtual photon is transverse in this region.

## I. INTRODUCTION

The study of nuclear effects on the structure functions measured in deep inelastic scattering (DIS) experiments at high energies is one of the main goals of high energy colliders and offers valuable information for understanding the dynamics of partons in the nuclear environment [1]. In the collinear factorized approach to pQCD, the partonic structure of bound nuclei is described by nuclear parton distribution functions (nPDFs) [2–4]. nPDFs are interesting in the transition between linear and non-linear (e.g., saturation) scale evolution of the parton densities [5]. Saturation occurs at low  $x$  and low interaction scale  $Q^2$  where the recombination of low- $x$  gluons becomes increasingly important. The transition line between the linear and non-linear regimes of the QCD dynamics is described by the saturation scale  $Q_s$ , which is predicted to depend on  $x$  and atomic number  $A$ . Increasing  $Q_s$  at smaller values of  $x$  and larger values of  $A$  will be a scenario to determine whether parton distributions saturate or not and allow us to disentangle non-linear from linear physics.

Taking into account non-linear effects that are inherent to the QCD dynamics at high energies when the hadron becomes a dense system can be quite well described by models based on Color Glass Condensate (CGC) formalism [6]. The nuclear saturation effect demonstrates that at small values of  $x$ , the gluon distribution in a nucleus is less than the gluon distribution in a nucleon. Such non-linearities are predicted to be more pronounced in lepton-nucleus than in lepton-proton scattering which is the key physics goal of an Electron-Ion Collider (EIC). Nuclear physics with electron-nucleus (eA) collisions can be explored at the EIC, where the maximum energy envisioned for electron-heavy ion runs would be achieved by colliding 18 GeV electrons with 110 GeV ions for a  $\sqrt{s} = 89$  GeV in the EIC Conceptual Design Report [7]. Indeed, the EIC, which is expected to begin science operations at Brookhaven National Laboratory in the early 2030s, promises to revolutionize our understanding of the internal structure of hadrons. The longitudinal proton structure function  $F_L$  at EIC through a Rosenbluth separation method with impacts of differing assumptions on sample sizes, systematic uncertainties and beam energy scenarios are investigated in Refs.[8, 9]. In Ref.[10] a factorized expression of the differential cross-section for single-inclusive jet production, for a longitudinally polarized photon, in terms of transverse momentum dependent (TMD) quark and gluon fracture functions is derived and shown that the quark TMD fracture function is the most sensitive to saturation effects in large nuclei.

The longitudinal structure function behavior on photon virtuality  $Q^2$  at fixed energy within the color dipole formalism for models considering parton saturation effects which resum a wide class of higher-twist (HT) contributions is considered in Ref.[11] based on the gluonic structure. The gluonic structure of light nuclei that exclusive vector

---

\*Electronic address: boroun@razi.ac.ir

meson production can provide, as well as the  $x$  dependence of coherent and incoherent cross sections at the EIC are considered in [12].

In the Operator Product Expansion (OPE), the scattering amplitudes are expanded into a series of contributions  $\sigma = \sum_{\tau} \sigma_{\tau}(Q^2)$ , with  $Q^2$  being the characteristic hard scale,  $\sigma_{\tau} \propto 1/Q^{\tau}$  and  $\tau = 2, 4, 6$  and  $8$  being the twist<sup>1</sup> [13]. Indeed, the higher twist corrections refer to a certain class of contributions to hard processes in strong interactions that are suppressed by a power of the hard scale. The influence of higher twist corrections to deep inelastic structure functions in the low- $Q^2$  and small- $x$  HERA region is investigated in Ref.[16]. A twist analysis of the saturation model describing the structure function and the DIS diffractive cross section at HERA is performed in [16]. In Ref.[17], the impact of the higher-twist effects resummed by the non-linear approaches for the QCD dynamics on the inclusive observable in EIC is investigated.

In this paper, the behavior of the ratio  $\frac{\sigma_{\tau}}{F_2}(A, x_{\min}, Q^2)$  due to the HT corrections at high inelasticity  $y = 1$  in the EIC COM energy in a wide range of the mass number  $A$  is considered. In Refs.[18, 19], the behavior of the DIS structure functions at high inelasticity, which is considered at the minimum value of  $x$  given by  $Q^2/s$  where the polarization of the exchanged photon is described to be transverse and the longitudinal structure function is expected to be small at this kinematic domain.

## II. METHOD

In the saturation model, the  $\gamma^*A$  – cross sections are defined in terms of the dipole cross section  $\hat{\sigma}(x, r^2)$  which describes the interaction of the  $q\bar{q}$  dipole pair with the nuclei by the gluonic field, as well as the transverse and longitudinally polarized photon wave functions  $\Psi_{T,L}(z, r)$  by the following formula:

$$\sigma_{T,L}(A, x, Q^2) = \int d^2\mathbf{r} \int dz \int d^2\mathbf{b} |\Psi_{T,L}(z, \mathbf{r}, Q^2)|^2 \hat{\sigma}(x, r^2) S(\mathbf{b}), \quad (1)$$

where

$$F_{T,L}(A, x, Q^2) = = \frac{Q^2}{4\pi^2\alpha_{em}} \sigma_{T,L}(A, x, Q^2). \quad (2)$$

The dipole cross section grows quadratically at small  $r$  and saturates at large  $r$ , where  $r$  is the relative transverse separation between quark and anti-quark. Here,  $z$  is the momentum fraction of the photon carried by the quark or anti-quark in the color dipole and  $\mathbf{b}$  is the transverse distance from the center of the nucleus to the center of mass of the  $q\bar{q}$  dipole [20].  $S(\mathbf{b})$  is the profile function in impact parameter space, usually described by a Wood-Saxon distribution. The Mellin transform of the wave functions from the dipole cross section to evaluate the cross sections in Eq. (1) is conducted in Ref.[16]. The transverse cross section has a double pole that generates a logarithmic behavior for the leading-twist contribution, while the longitudinal leading-twist contribution has only a single pole. Higher-twist contributions are obtained by evaluating the residues at the lower lying poles in [16].

The transverse and longitudinal structure functions are calculated [16, 17] by expanding in powers of  $\xi_A \equiv Q_{s,A}^2/Q^2$ , where  $Q_{s,A}$  represents the saturation scale for the nucleus. It is defined as  $Q_{s,A}^2 = A^{1/3} Q_0^2 (x_0/x)^{\lambda}$  with  $Q_0^2 = 1 \text{ GeV}^2$ . In electron-ion collisions, the target area and the transverse size of the dipole cross section scale with  $S \rightarrow S_A = A^{2/3} S$ . The transverse and longitudinal structure functions at a fixed  $\sqrt{s}$  and  $Q^2$  at  $x_{\min} = Q^2/s$  can be expressed in terms of the parameter  $\xi_A$  modified as  $\xi_A \rightarrow \xi'_A = A^{1/3} \frac{Q_0^2}{Q^2} (\frac{sx_0}{Q^2})^{\lambda}$ . This limit is crucial as it describes the polarization of the exchanged photon as transverse, with the longitudinal structure function expected to be small. At low values of  $x$ , the dominant gluon component in the longitudinal structure function is strongly suppressed [18, 19]. Therefore, we have

$$F_k^{\tau}(A, Q^2/s, Q^2) = \frac{Q^2}{4\pi^2\alpha_{em}} A^{2/3} \sigma_0 \sum e_f^2 \frac{\alpha_{em}}{\pi} \sum_{n=2} \eta_n^k \xi_A^{n/2} \quad \text{with } n = \tau \text{ even and } k = T, L, \quad (3)$$

---

<sup>1</sup> The notion of twist was introduced in 1971 in the paper by Gross and Treiman [14] who noticed that "it is no longer the dimension alone that determines the importance of an operator near the light-cone, but rather the difference between the dimension and spin". They called this quantity the "twist" on an operator  $\tau$  with the original definition  $\tau = \text{dimension} - \text{spin}$  is sometimes referred to as "geometric twist". [15].

where  $n$  indicates the twist-2, 4, 6 and 8 analysis. The coefficient functions  $\eta_n$  according to Refs.[16, 17] are:

$$\begin{aligned}
\eta_2^L &= 1 \\
\eta_2^T &= \frac{7}{6} - \psi(2) + \ln\left(\frac{1}{\xi'_A}\right) \\
\eta_4^L &= -\frac{94}{75} + \frac{4}{5}\psi(3) - \frac{4}{5}\ln\left(\frac{1}{\xi'_A}\right) \\
\eta_4^T &= \frac{6}{10} \\
\eta_6^L &= \frac{654}{1225} - \frac{36}{35}\psi(4) + \frac{36}{35}\ln\left(\frac{1}{\xi'_A}\right) \\
\eta_6^T &= \frac{43}{1225} - \frac{12}{35}\psi(4) + \frac{12}{35}\ln\left(\frac{1}{\xi'_A}\right) \\
\eta_8^L &= -\frac{1636}{18375} + \frac{48}{175}\psi(5) - \frac{48}{175}\ln\left(\frac{1}{\xi'_A}\right) \\
\eta_8^T &= -\frac{262}{11025} + \frac{4}{35}\psi(5) - \frac{4}{35}\ln\left(\frac{1}{\xi'_A}\right).
\end{aligned} \tag{4}$$

The inclusive  $eA$  scattering cross-section at low  $Q^2$  and  $x$  at EIC will be bounded due to kinematic factors. The cross-section in reduced form is given by

$$\begin{aligned}
\frac{\sigma_r}{F_2}(A, Q^2/s, Q^2) &= 1 - \frac{F_L}{F_2}(A, Q^2/s, Q^2) = 1 - \frac{F_L}{F_T + F_L}(A, Q^2/s, Q^2) = \left[1 + \frac{F_L^T}{F_T^T}(A, Q^2/s, Q^2)\right]^{-1} \\
&= \left[1 + \frac{\sum_\tau \eta_\tau^L \xi_A'^{n/2}}{\sum_\tau \eta_\tau^T \xi_A'^{n/2}}\right]^{-1}.
\end{aligned} \tag{5}$$

The dipole cross-section depends on  $x$  and  $r$  according to [21, 22]

$$\int d^2\mathbf{b} \hat{\sigma}(x, r^2) S(\mathbf{b}) = 2[1 - \exp(-r^2 Q_{s,A}^2/4)] \int d^2\mathbf{b} S(\mathbf{b}) = A^{2/3} \sigma_0 [1 - \exp(-r^2 Q_{s,A}^2/4)]. \tag{6}$$

In the color dipole model (CDM), the cross section in reduced form is:

$$\frac{\sigma_r}{F_2}(A, Q^2/s, Q^2) = 1 - \frac{\int d^2\mathbf{r} \int dz |\Psi_L(z, \mathbf{r}, Q^2)|^2 [1 - \exp(-r^2 Q_{s,A}^2/4)]}{\int d^2\mathbf{r} \int dz \{|\Psi_T(z, \mathbf{r}, Q^2)|^2 + |\Psi_L(z, \mathbf{r}, Q^2)|^2\} [1 - \exp(-r^2 Q_{s,A}^2/4)]}, \tag{7}$$

where  $Q_{s,A}^2 = A^{1/3} Q_0^2 (sx_0/Q^2)^\lambda$ . In Eq. (7),  $\Psi_{L,T}$  represent the spin-averaged light-cone wave functions of the photon. The square of the photon wave function indicates the probability of a  $(q\bar{q})$  fluctuation occurring with a transverse size relative to the photon polarization. The light-cone photon wave function,  $\Psi$ , is represented by the lowest order  $\gamma^* g \rightarrow q\bar{q}$  scattering amplitudes which give

$$|\Psi_T^f(z, r, Q^2)|^2 = \frac{2N_c \alpha_{em} e_f^2}{4\pi^2} \left\{ [z^2 + (1-z)^2] \epsilon^2 K_1^2(\epsilon r) + m_f^2 K_0^2(\epsilon r) \right\} \tag{8}$$

and

$$|\Psi_L^f(z, r, Q^2)|^2 = \frac{8N_c \alpha_{em} e_f^2}{4\pi^2} Q^2 z^2 (1-z)^2 K_0^2(\epsilon r), \tag{9}$$

where  $\epsilon^2 = z(1-z)Q^2 + m_f^2$ ,  $K_0$  and  $K_1$  are modified Bessel functions, and the sum is over quark flavors  $f$  with quark mass  $m_f$ .

In the following the validity of the higher-twist corrections to the nuclear reduced cross section with respect to the EIC COM energy at the critical points between the linear and non-linear regimes according to the high inelasticity due to the  $\xi'_A$  variable, will be investigated.

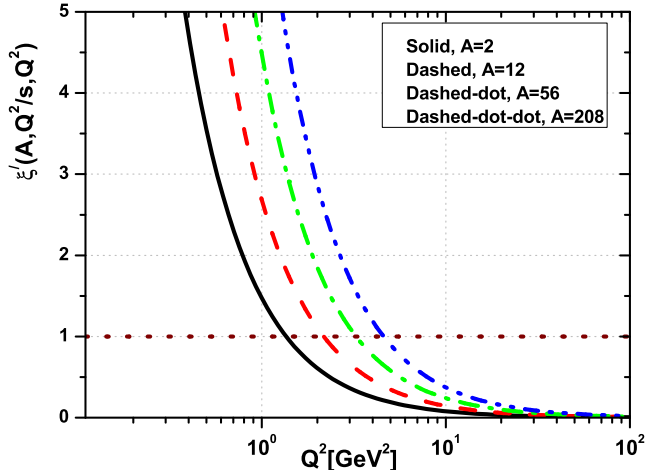


FIG. 1: Linear ( $\xi'_A \lesssim 1$ ) and non-linear ( $\xi'_A > 1$ ) regions are plotted as a function of  $Q^2$  and nuclear mass number  $A$  for  $n_f = 3$ , according to the transition point  $\xi'_A \approx 1$  (short-dashed-brown line). The curves represent (Deuterium-2 (solid-black curve), Carbon-12 (dashed-red curve), Fe-56 (dashed-dot-green curve), and Lead-208 (dashed-dot-dot-blue curve) at the EIC COM energy with  $\sqrt{s} = 89$  GeV.

### III. RESULTS AND CONCLUSION

The transition point between the linear and non-linear regimes occurs when  $\xi'_A \approx 1$  and is proportional to the mass number  $A$  and the  $Q^2$  variable at a fixed  $\sqrt{s}$  and high inelasticity. The perturbative region is proportional to the linear region with  $\xi'_A \lesssim 1$  at large  $Q^2$ . At small  $Q^2$ , the nonperturbative region with  $\xi'_A > 1$  is proportional to the non-linear region defined by the Pomeron region [16]. In Fig.1 the linear and non-linear regions are shown due to the large and small values of  $\xi'_A$  at the limit  $x_{\min} = Q^2/s$  according to the EIC collider with COM energy of  $\sqrt{s} = 89$  GeV for  $n_f = 3$  is shown. The theoretical expectations for the transition point are obtained using the parameters  $Q_0^2 = 1$  GeV<sup>2</sup>,  $\sigma_0 = 23.58$  mb,  $\lambda = 0.270$ ,  $x_0 = 2.24 \times 10^{-4}$ , and  $m_f = 0.14$  GeV [23] in Fig.1. The critical point increases towards large  $Q^2$  values as the mass number  $A$  increases. These critical points, which indicate the boundary between the linear and non-linear regimes, are approximately obtained for Deuterium-2, Carbon-12, Fe-56, and Lead-208 at the  $Q^2$  values  $Q^2 \lesssim 2, 3, 4,$  and  $6$  GeV<sup>2</sup>.

In Fig.2, the contributions of distinct twists to the ratio  $\frac{\sigma_r}{F_2}(A, Q^2/s, Q^2)$  for various nuclei across a wide range of  $Q^2$  values at the EIC COM energy with  $\sqrt{s} = 89$  GeV and  $x_{\min} = Q^2/s$  for  $n_f = 3$  are analyzed and compared with the GBW model. It is observed that the distinct twists exhibit similar behavior at large values of  $Q^2$ , with the ratio  $\frac{\sigma_r}{F_2} < 1$  at this limit being independent of the twists and the increasing mass number  $A$ . The full results with the GBW model show that the ratio  $\frac{\sigma_r}{F_2}(A, Q^2/s, Q^2) = 1$  at large values of  $Q^2$ . The intersection point between the GBW model and twist-2+4 indicates the critical point between the linear and non-linear regimes in Fig.2. This point shifts towards larger  $Q^2$  values as the mass number  $A$  increases. The effects of twist-6 and twist-8 at low  $Q^2$  values are more noticeable. The ratio  $\frac{\sigma_r}{F_2} \rightarrow 1$  at low  $Q^2$  values in the GBW model and higher twist corrections, as the longitudinal structure function is approximately  $F_L \rightarrow 0$  as  $Q^2 \rightarrow 0$ , indicating that the polarization of the exchanged photon is transverse. The ratio from the GBW model is larger than the higher twist corrections at both small and large values of  $Q^2$ .

The impact of higher twist corrections on  $\frac{\sigma_r}{F_2}(A, Q^2/s, Q^2)$  is minimal at large  $Q^2$  values, which also holds true for larger values of  $A$ . However, the main difference is that the impact of higher twist corrections becomes significant at small values of  $Q^2$ . The ratio is significantly influenced by the twist-4+6+8 terms, which provide substantial positive corrections to the leading-twist contribution at low  $Q^2$ . The disparity between the higher twist corrections (i.e., twist-2, twist-2+4, twist-2+4+6 and twist-2+4+6+8) and the full predictions from the GBW model for the ratio  $\frac{\sigma_r}{F_2}(A, Q^2/s, Q^2)$  diminishes to less than 8.8% with Lead-208 and 7.7% with Deuterium-2 for large  $Q^2$  values.

For comparison with experimental data, we calculated the ratio  $\frac{F_L}{F_2}(A, x, Q^2)$  for deuterium and compared it with

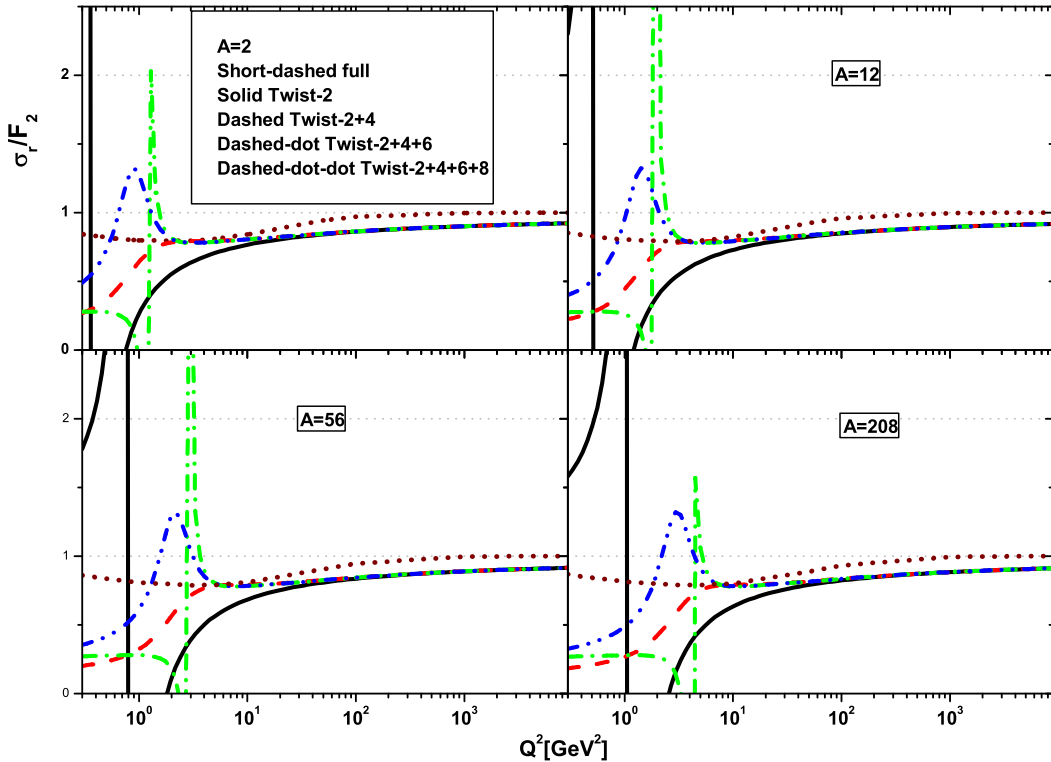


FIG. 2: The higher-twist corrections, including twist-2 (solid-black curve), twist-2+4 (dashed-red curve), twist-2+4+6 (dashed-dot-green curve), and twist-2+4+6+8 (dashed-dot-dot-blue curve), to the ratio  $\frac{\sigma_L}{F_2}$  at the EIC COM energy with  $\sqrt{s} = 89$  GeV with  $x_{\min} = Q^2/s$  are compared with the GBW model (short-dashed-brown full curve) for  $n_f = 3$  and nuclei Deuterium-2, Carbon-12, Fe-56, and Lead-208.

the results obtained at Jefferson Lab (JLab) [24] in Fig.3. The error bars of the ratio  $F_{L2} \equiv \frac{F_L}{F_2}$  in the JLab data are determined by the following formula:

$$\Delta(F_{L2}) = F_{L2} \sqrt{(\Delta F_L/F_L)^2 + (\Delta F_2/F_2)^2},$$

where in the JLab data,  $\Delta F_L$  and  $\Delta F_2$  are taken from the JLab E00-002 [24]. The parameter  $\xi'_A$  for the results of the ratio  $\frac{F_L}{F_2}(A = 2, x, Q^2)$  indicates that the data from JLab are in the linear region when  $\xi'_A \leq 1$  for  $x > 0.02$  at  $Q^2 = 0.4$  GeV<sup>2</sup>. In Fig.3, the ratio  $\frac{F_L}{F_2}$  for deuterium is determined at  $Q^2 = 0.4$  GeV<sup>2</sup> for  $n_f = 3$  to account for higher twist corrections and compared with the results from JLab and the CDM<sup>2</sup>. We observe that the data in the linear regime with twists-(2+4, 2+4+6 and 2+4+6+8) are comparable to the JLab data, showing a significant negative correction to the leading twist contribution. The JLab data in Fig.3 approaches  $\frac{F_L}{F_2} \rightarrow 0$  as the higher twist corrections from twist-6 and twist-8 at low  $Q^2$  values indicate that the polarization of the virtual photon is transverse when the longitudinal structure function approaches low  $x$  values. We conclude that the results at low  $Q^2$  values with twist-4 strongly influence the results in the linear region, valid for  $\xi'_A \lesssim 1$ , while twist-6 and twist-8 affect the saturation region where  $Q_{s,A}^2 \geq Q^2$  and non-linear effects amplify and modify the observables at low  $Q^2$  and  $x$  values in the EIC.

<sup>2</sup> For further discussion, refer to Appendix A.

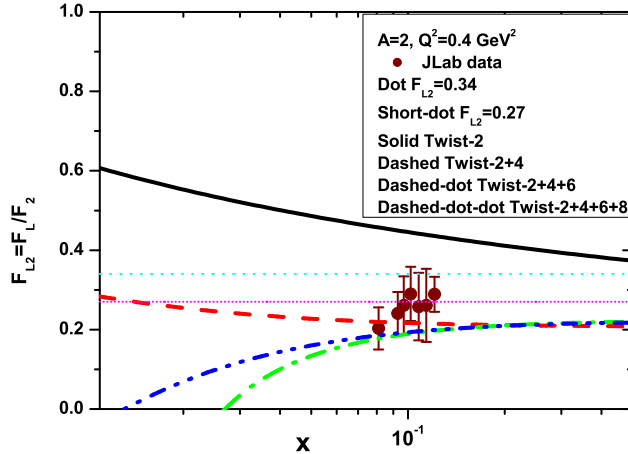


FIG. 3: The extracted ratio  $F_{L2}$  of Deuterium in the twist expansion for twist2 (solid-black curve), twist-2+4 (dashed-red curve), twist-2+4+6 (dashed-dot-green curve) and twist-2+4+6+8 (dashed-dot-dot-blue curve) as a function of  $x$  is plotted at  $Q^2 = 0.4 \text{ GeV}^2$  at the active flavor numbers  $n_f = 3$  and compared with the data from JLab E00-002 [24] (shown as brown points). The results are compared to the dipole upper bounds by lines corresponding to  $F_{L2} = 0.27$  (short-dot-magenta line) and  $F_{L2} = 0.34$  (dot-cyan line).

In conclusion, we have examined the behavior of the ratio  $\frac{\sigma_r}{F_2}(A, Q^2/s, Q^2)$  for light and heavy nuclei at  $y = 1$ , where  $x_{Bj} = x_{\min} = Q^2/s$ , in the EIC kinematics. We utilized the CDM and the twist expansion for low  $x$  in this scenario. Our model provides a good description of results at moderate and large  $Q^2$  values and predicts nuclear ratio  $\frac{\sigma_r}{F_2}(A, Q^2/s, Q^2)$  that can be measured in electron-ion collisions at  $x_{\min}$ . These results at moderate and large  $Q^2$  values strongly suggests that the gluon component is the dominant factor in the longitudinal structure function within the dipole picture. We observed that the value of  $F_L$  is small at low  $Q^2$  values in the dipole picture. This is because the dominant gluon component is strongly suppressed and the polarization of the exchanged photon is transverse at this kinematic point. We investigated the nuclear ratio  $\frac{\sigma_r}{F_2}(A, Q^2/s, Q^2)$  at this limit, which reveals high gluon densities and associated nonlinear high-energy evolution. The non-linear corrections at the saturation regime increase with the mass number  $A$ . The ratio  $\frac{F_{L2}^A}{F_2^A}$  can serve as an indicator for the presence of non-linear low  $x$  dynamics in large nuclei. The ratio of  $F_{L2}$  for deuterium at low four-momentum transfer squared is determined and compared with the JLab E00-002 data and the CDM bounds. Indeed, the search for non-linear effects in light and heavy nuclei based on the EIC kinematics is investigated because the non-linear regime is enhanced by a factor  $\propto A^{1/3}$ , the nuclear saturation scale as this approaches resums higher twist contributions at low  $Q^2$  as observed in Refs.[16, 17].

## APPENDIX A

In Refs.[25, 26, 28], the authors demonstrate that at large  $Q^2$ , the ratio of photo absorption cross sections is determined by a parameter  $\rho$ , which describes the dissociation of photons into  $q\bar{q}$  pairs,  $\gamma_{L,T}^* \rightarrow q\bar{q}$ , with the reaction:

$$R = \frac{1}{2\rho}, \quad (10)$$

where the factor 2 in the equation originates from the difference in the photon wave functions. Essentially, the  $\rho$  parameter represents the ratio of the average transverse momenta, given by:  $\rho = \frac{\langle \vec{k}_\perp^2 \rangle_L}{\langle \vec{k}_\perp^2 \rangle_T}$ , or it can be related to the ratio of the effective transverse sizes of the  $(q\bar{q})_{L,T}^{J=1}$  states as  $\frac{\langle \vec{r}_\perp^2 \rangle_L}{\langle \vec{r}_\perp^2 \rangle_T} = \frac{1}{\rho}$ . For the specific value of  $\rho = \frac{4}{3}$  in Ref.[26]

<sup>3</sup>, it is found that  $R = \frac{3}{8} = 0.375$  and the ratio of structure functions is  $F_{L2}(x, Q^2) = \frac{3}{11} = 0.273$ . When  $\rho = 1$  (i.e., helicity independent), the ratio is approximately 0.34, serving as an upper bound for  $F_{L2}(x, Q^2)$  in the dipole model. In Refs.[29–31], the authors establish that the ratio of structure functions in the dipole model is independent of the dipole cross section  $\sigma_{\text{dip}}$ , being proportional to the photon- $q\bar{q}$  wave function as

$$F_{L2}(x, Q^2) = g(Q, r, m_q) \leq \tilde{g}(z_m) = 0.27139, \quad (11)$$

where

$$g(Q, r, m_q) = \frac{\int_0^1 dz |\Psi_L(\mathbf{r}, z; Q^2)|^2}{\int_0^1 dz \left[ |\Psi_T(\mathbf{r}, z; Q^2)|^2 + |\Psi_L(\mathbf{r}, z; Q^2)|^2 \right]} \quad (12)$$

and  $m_q$  represents the mass of the active quark <sup>4</sup>. For massless quarks, the function  $g(Q, r, m_q)$  is defined by the dimensionless variable  $z = Qr$ , where the function  $\tilde{g}(z) = g(Q, r, 0)$  reaches its maximum at  $z_m = 2.5915$  with  $\tilde{g}(z) = 0.27139$ . Previous studies [32–35] have shown that the bound specified by Eq. (11) for the ratio of structure functions holds true for all  $Q \geq 0$ ,  $r \geq 0$  and  $m_q \geq 0$ .

- 
- [1] A. Accardi et al., *Eur. Phys. J. A* **52**, 268 (2016).  
[2] N.Armesto, H.Paukkunen, Carlos A.Salgado, and K.Tywniuk, *Phys.Lett.B* **694**, 38 (2010).  
[3] E.C.Aschenauer et al., *Phys. Rev. D* **96**, 114005 (2017).  
[4] N.Armesto et al., *Phys.Rev.D* **109**, 054019 (2024).  
[5] C. Marquet, M. R. Moldes, and P. Zurita, *Phys.Lett.B* **772**, 607 (2017).  
[6] J. Jalilian-Marian, A. Kovner, L. McLerran, and H. Weigert, *Phys. Rev. D* **55**, 5414 (1997); J. Jalilian-Marian, A. Kovner, and H. Weigert, *Phys. Rev. D* **59**, 014014 (1999), *ibid.* **59**, 014015 (1999), *ibid.* **59** 034007 (1999); A. Kovner, J. Guilherme Milhano, and H. Weigert, *Phys. Rev. D* **62**, 114005 (2000); H. Weigert, *Nucl. Phys. A* **703**, 823 (2002); E. Iancu, A. Leonidov, and L. McLerran, *Nucl.Phys. A* **692**, 583 (2001); E. Ferreiro, E. Iancu, A. Leonidov, and L. McLerran, *Nucl. Phys. A* **701**, 489 (2002).  
[7] F. Willeke, Report Number: BNL-221006-2021- FORE, DOI: 10.2172/1765663.  
[8] Javier J.Lopez, Paul R.Newman, and K.Wichmann, arXiv: 2412.16123.  
[9] P. Agostini et al. (LHeC Collaboration and FCC-he Study Group), *J. Phys. G* **48**, 110501 (2021).  
[10] P.Caucal and F.Salazar, *Phys. Rev. Lett.* 136, 081901 (2026).  
[11] M.V.T.Machado, *Eur. Phys. J. C* **47**, 365 (2006).  
[12] H.Mantysaari and B.Schenke, *Phys.Rev.C* **101**, 015203 (2020).  
[13] R. K. Ellis, W. Furmanski and R. Petronzio, *Nucl. Phys. B* **212**, 29 (1983).  
[14] D.J. Gross, S.B. Treiman, *Phys. Rev. D* **4**, 1059 (1971).  
[15] V.M.Braun, *EPJ Web of Conferences* 274, 01012 (2022).  
[16] J.Bartels, K.Golec-Biernat, and K.Peters, *Eur. Phys. J. C* **17**, 121 (2000).  
[17] Yan B. Bandeira and Victor P.Goncalves, *Eur. Phys. J. A* **59**, 19 (2023).  
[18] Frank E.Taylor, *Phys.Rev.D* **111**, 052001 (2025).  
[19] G.R.Boroun, *Phys.Rev.D* **112**, 074022 (2025).  
[20] N. N. Nikolaev and B. G. Zakharov, *Phys. Lett. B* **332**, 184 (1994); *Z. Phys. C* **64**, 631 (1994).  
[21] K. Golec-Biernat and M. Wusthoff, *Phys. Rev. D* **59**, 014017 (1999).  
[22] K. Golec-Biernat and M. Wusthoff, *Phys. Rev. D* **60**, 114023 (1999).  
[23] K. Golec-Biernat and S. Sapeta, *JHEP* **03**, 102 (2018).  
[24] V.Tvaskis et al., *Phys. Rev. C* **97**, 045204 (2018).  
[25] G. Cvetic, D. Schildknecht, B. Surrow and M. Tentyukov, *Eur. Phys. J. C* **20**, 77 (2001) .  
[26] M. Kuroda and D. Schildknecht, *Phys. Lett. B* **618**, 84 (2005); *Phys. Lett. B* **670**, 129 (2008); *Phys. Rev. D* **85**, 094001 (2012); *J. Mod. Phys. A* **31**, 1650157 (2016) .  
[27] G.R.Boroun, M. Kuroda and D. Schildknecht, *Eur. Phys. J. Plus* **140**, 1149 (2025); arXiv [hep-ph]: 2407.03708.  
[28] D. Schildknecht and M. Tentyukov, arXiv[hep-ph]:0203028, Report number: BI-TH 2002/04.  
[29] C. Ewerz, A. von Manteuffel and O. Nachtmann, *Phys.Rev.D* **77**, 074022 (2008) .

---

<sup>3</sup> For further discussion, readers can refer to the papers by M. Kuroda and D. Schildknecht: "Phys. Rev. D 85 (2012) 094001" and "J. Mod. Phys. A 31 (2016) 1650157".

<sup>4</sup> For further discussion see [30].

- [30] C. Ewerz, A. von Manteuffel, O. Nachtmann and A. Schoning, *Phys.lett.B* **720**, 181 (2013).
- [31] C. Ewerz, O. Nachtmann, *Phys.Lett.B* **648**, 279 (2007).
- [32] B.Rezaei and G.R.Boroun, *Phys.Rev.C* **101**, 045202 (2020) .
- [33] M. Niedziela and M. Praszalowicz, *Acta Physica Polonica B* **46**, 2018 (2015).
- [34] G.R.Boroun and B.Rezaei, *Phys.Rev.C* **103**, 065202 (2021); *Nucl.Phys.A* **990**, 244 (2019).
- [35] G.R.Boroun, *Eur.Phys.J.A* **57**, 219 (2021); *Phys.Rev.D* **109**, 054012 (2024).